

Accuracy Simulation of MF R-Mode Systems Using TOA Variance

Jaewon Yu
School of Integrated Technology
Yonsei University
Incheon, Korea
jaewon.yu@yonsei.ac.kr

Pyo-Woong Son*
Department of Electronics Engineering
Chungbuk National University
Cheongju, Korea
pwson@cbnu.ac.kr
* Corresponding author

Abstract—To ensure consistent navigation services despite GNSS signal disruptions, Korea is developing the R-Mode system. This study focuses on enhancing the simulation accuracy of the MF R-Mode system’s performance by integrating data from the Eocheong transmitter with existing data from the Palmi and Chungju transmitters. Additional measurements from these three transmitters were gathered using the DARBS receiver to model the Time-of-Arrival (TOA) variance. Analysis of this data facilitated the calculation of new constants and transmitter-specific jitter values, which were then used to determine coverage areas based on the updated parameters.

Index Terms—Medium-frequency (MF) R-Mode system, time-of-arrival (TOA) measurements, variance modeling, coverage

I. INTRODUCTION

Global Navigation Satellite Systems (GNSS) [1]–[9] provide highly accurate positioning, navigation, and timing (PNT) information by receiving signals transmitted from satellites. However, these signals are vulnerable to radio frequency interference (RFI) [10]–[16] and ionospheric anomalies [17]–[23]. North Korea has conducted several GPS jamming attacks, impacting various sectors including maritime, communication, and aviation in South Korea. [24]–[27].

To ensure stable and independent navigation services as a backup to GPS, South Korea is considering the eLoran system [24], [28], [29]. Based on the Loran-C system, eLoran provides PNT services by transmitting powerful signals from multiple ground-based transmitters. From 2016 to 2020, South Korea developed eLoran technology, establishing a time synchronization system at the existing Pohang and Gwangju transmitters and installing a low-power transmitter at the Incheon test site. In 2023, the Incheon test site’s low-power transmitter was relocated to Socheong Island in the northern West Sea, increasing the effective radiated power to 8 kW. Currently,

This work was supported in part by Grant RS-2024-00407003 from the “Development of Advanced Technology for Terrestrial Radionavigation System” project, funded by the Ministry of Oceans and Fisheries, Republic of Korea; in part by the National Research Foundation of Korea (NRF), funded by the Korean government (Ministry of Science and ICT), under Grant RS-2024-00358298; in part by the Future Space Navigation and Satellite Research Center through the NRF, funded by the Ministry of Science and ICT (MSIT), Republic of Korea, under Grant 2022M1A3C2074404; and in part by the MSIT, Korea, under the Information Technology Research Center (ITRC) support program supervised by the Institute of Information & Communications Technology Planning & Evaluation (IITP) under Grant IITP-2024-RS-2024-00437494.

Korea’s eLoran system consists of three main transmitters (Pohang, Gwangju, Socheong Island) and two differential Loran stations (Incheon, Pyeongtaek), providing a foundation for reliable navigation services even in GPS signal interference situations [27].

Recently, Korea has sought to reduce the high initial installation costs of eLoran transmitters by upgrading its communication infrastructure [30], [31]. This effort includes leveraging Medium Frequency (MF) and Very High Frequency (VHF) signals as part of the R-Mode project, which can cover a wider area by utilizing the already existing infrastructure. Studies have been conducted to determine the parameters necessary for calculating signal strength and to apply these parameters in simulation tools to model the signal strength of the Yeongju transmitter [32]. Additionally, research has been undertaken to model the variance in Time of Arrival (TOA) measurements using data collected from the Palmi and Chungju transmitters [33]. However, these studies were limited to data from only two transmitters, making it difficult to accurately assess the system’s overall performance.

In this paper, we enhance the modeling of TOA variance by integrating additional measurements, including data from the Eocheong transmitter. By incorporating these new data, we improve the accuracy of system performance calculations, overcoming previous limitations and resulting in more precise simulation outcomes. Data were gathered using the DARBS receiver, and the parameters for the Eocheong, Palmi, and Chungju transmitters were re-estimated by integrating these new data into the previous research datasets. (More details about the receiver can be found at <https://darbs.co.kr/>.) A coverage map created using the combined data from the three transmitters was produced to evaluate system performance.

II. METHODOLOGY

A. Estimation of Parameters for MF R-Mode TOA Measurements

The TOA variance formula for the MF R-Mode system follows [33]:

$$\sigma_i^2 = J_i^2 + \frac{C^2}{SNR_i} \quad (1)$$

Jitter refers to random errors originating from the transmitter and is independent of the receiver's location, caused by thermal noise and other reasons [25], [34]. J_i represents the jitter of transmitter i , and C is a constant value, both of which are parameters estimated from actual measurement data. σ denotes the standard deviation of the MF R-Mode TOA measurements, while SNR_i represents the signal-to-noise ratio of the signal received from transmitter i . The constants C and jitter values in 1 are parameters that can be updated as new data is incorporated.

B. Data Collection and Processing

In this research, alongside the data obtained from [33], we use raw phase measurements and SNR data collected using the DARBS medium frequency receiver from Palmi, Chungju, and Eocheong in Korea. The SNR data is taken from the receiver's measurements, and the formula for calculating σ_i^2 from the raw phase measurements follows [33]:

$$\sigma_i^2 = \text{Var}(\text{TOA}_i) = \left(\frac{\lambda}{2\pi}\right)^2 \cdot \text{Var}(\phi_{\text{cont},i}) \quad (2)$$

Here, λ denotes the wavelength of the CW signal. The parameters J_i and C are derived by minimizing the residual sum of squares (RSS) between the model in (2) and the actual measurements, based on the observed SNR_i and σ_i^2 values.

C. Accuracy Calculation of MF R-Mode

The approach for determining the signal accuracy follows the same procedure as outlined in [25], [34]. All equations in this section are from [25].

The geometry matrix G , which is detailed in (3), is constructed using the sine and cosine of the angles between the user and each transmitter, θ_i .

$$G = \begin{bmatrix} \cos(\theta_1) & \sin(\theta_1) & 1 \\ \cos(\theta_2) & \sin(\theta_2) & 1 \\ \cos(\theta_3) & \sin(\theta_3) & 1 \end{bmatrix} \quad (3)$$

The matrix R , which is based on the variances σ_i^2 , is defined as follows:

$$R = \begin{bmatrix} \sigma_1^2 & 0 & 0 \\ 0 & \sigma_2^2 & 0 \\ 0 & 0 & \sigma_3^2 \end{bmatrix} \quad (4)$$

Using this matrix, the error covariance matrix K for the position estimation is determined by (5).

$$K = (G^T R^{-1} G)^{-1} \quad (5)$$

The 95% horizontal accuracy is derived using the error covariance matrix for the position estimation, as shown in (6).

$$\text{Accuracy} = 2\sqrt{K_{11} + K_{22}} \quad (6)$$

K_{11} and K_{22} are the diagonal components of the error matrix, indicating the variance in the position estimation. The accuracy calculation assumes the position solution is unbiased

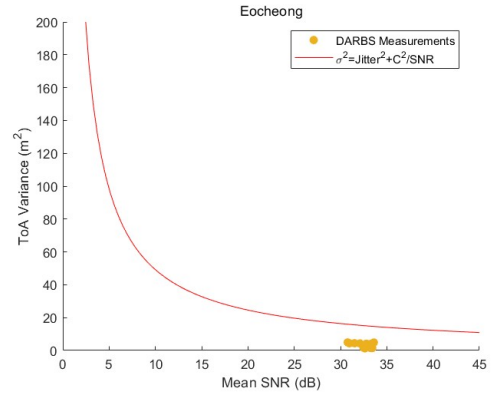


Fig. 1. Model fit for Eocheong transmitter. Yellow points represent measurements from the DARBS receiver and the red curve represents (1).

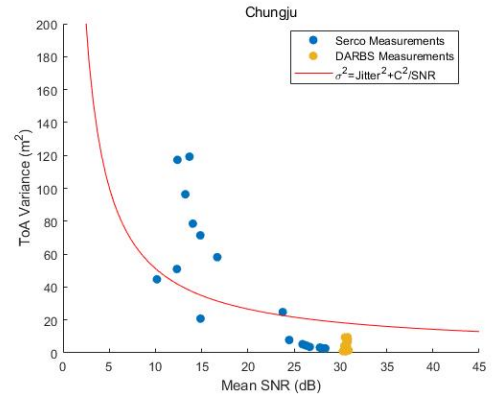


Fig. 2. Model fit for Chungju transmitter. Yellow points represent measurements from the DARBS receiver, blue points represent measurements from the Serco receiver, and the red curve represents (1).

and that biases from ASF are corrected through spatial and temporal ASF adjustments. This type of accuracy is known as repeatable accuracy.

III. RESULTS

A. Results of MF R-Mode Parameter Estimation

Fig. 1, Fig. 2 and Fig. 3 show the fit of the model to the actual measurements for Eocheong, Chungju and Palmi transmitters. The yellow points denote the empirical data collected using the DARBS receiver, while the blue points represent the data measured using the Serco receiver as used in [33]. The x-axis shows SNR_i , and the y-axis displays the TOA variance (σ_i^2). The model, represented by the red curve, is (1). The estimated values are as follows: the jitter value for Palmi is 0.00, for Chungju is 1.41, for Eocheong is 0.00, and the C value is 22.15. Based on these values, σ_i^2 can be predicted for each transmitter's SNR_i .

B. MF R-Mode Coverage Map

Table I lists the input parameters utilized in the simulation. Using the specified input parameters, the simulation generated the coverage map presented in Fig. 4. This map visually

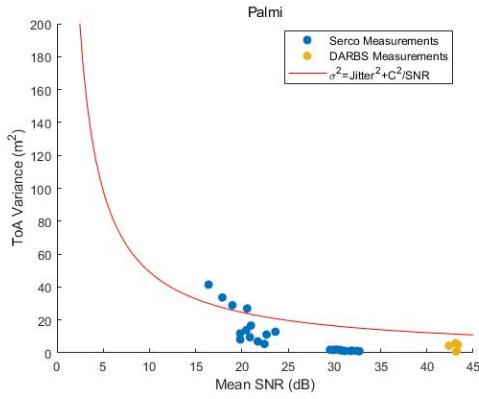


Fig. 3. Model fit for Palmi transmitter. Yellow points represent measurements from the DARBS receiver, blue points represent measurements from the Serco receiver, and the red curve represents (1).

TABLE I
SIMULATION INPUT PARAMETERS

Simulation Input Parameters	Settings
Eocheong Transmitter Power	300W
Palmi Transmitter Power	300W
Chungju Transmitter Power	500W
Eocheong Transmitter Jitter	0m
Palmi Transmitter Jitter	0m
Chungju Transmitter Jitter	1.41m
Season	'Averaged'
Noise Level	95%
SNR Threshold	-15dB

represents the coverage calculated based on the transmitter locations and the signal strength at each location.

IV. CONCLUSION

This study has enhanced the modeling of MF R-Mode TOA variance by incorporating additional data from the Eocheong transmitter alongside the Palmi and Chungju transmitters. By re-estimating jitter parameters for all three transmitters, we

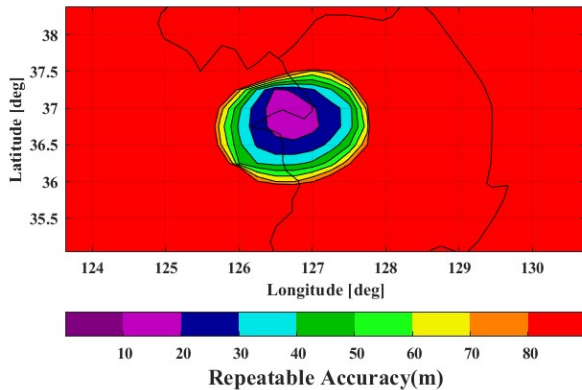


Fig. 4. Coverage map of the MF R-Mode system.

improved the system's repeatability accuracy and generated a comprehensive coverage map. A constraint of this research is its inability to fully consider time-variant factors such as changes in atmospheric noise. This is because different receivers experience varying levels of internal noise and receive signals at different times. Future research should address this limitation to improve the accuracy of the model. These efforts advance the simulation tools and contribute to the ongoing development of the R-Mode system in Korea.

REFERENCES

- [1] M. Kim, J. Seo, and J. Lee, "A comprehensive method for GNSS data quality determination to improve ionospheric data analysis," *Sensors*, vol. 14, no. 8, pp. 14971–14993, Aug. 2014.
- [2] Y.-H. Chen, J.-C. Juang, D. De Lorenzo, J. Seo, S. Lo, P. Enge, and D. Akos, "Real-time dual-frequency (L1/L5) GPS/WAAS software receiver," in *Proc. ION GNSS*, 2011, pp. 767–774.
- [3] Y. Lee, Y. Hwang, J. Y. Ahn, J. Seo, and B. Park, "Seamless accurate positioning in deep urban area based on mode switching between DGNSS and multipath mitigation positioning," *IEEE Trans. Intell. Transp. Syst.*, vol. 24, no. 6, pp. 5856–5870, Jun. 2023.
- [4] S. Kim and J. Seo, "Machine-learning-based classification of GPS signal reception conditions using a dual-polarized antenna in urban areas," in *Proc. IEEE/ION PLANS*, Apr. 2023, pp. 113–118.
- [5] W. Kim and J. Seo, "Low-cost GNSS simulators with wireless clock synchronization for indoor positioning," *IEEE Access*, vol. 11, pp. 55 861–55 874, 2023.
- [6] H. Lee, S. Kim, J. Park, S. Jeong, S. Park, J. Yu, H. Choi, and J. Seo, "A survey on new parameters of GPS CNAV/CNAV-2 and their roles," *J. Position. Navig. Timing*, vol. 13, no. 1, pp. 45–52, 2024.
- [7] S. Kim, S. Park, and J. Seo, "Single antenna based GPS signal reception condition classification using machine learning approaches," *J. Position. Navig. Timing*, vol. 12, no. 2, pp. 149–155, 2023.
- [8] S. Kim, J. Byun, and K. Park, "Machine learning-based GPS multipath detection method using dual antennas," in *Proc. ASCC*, May 2022, pp. 691–695.
- [9] H. Lee, J. Seo, and Z. Kassas, "Urban road safety prediction: A satellite navigation perspective," *IEEE Intell. Transp. Syst. Mag.*, vol. 14, no. 6, pp. 94–106, Nov.-Dec. 2022.
- [10] K. Park and J. Seo, "Single-antenna-based GPS antijamming method exploiting polarization diversity," *IEEE Trans. Aerosp. Electron. Syst.*, vol. 57, no. 2, pp. 919–934, Apr. 2021.
- [11] K. Park, D. Lee, and J. Seo, "Dual-polarized GPS antenna array algorithm to adaptively mitigate a large number of interference signals," *Aerosp. Sci. Technol.*, vol. 78, pp. 387–396, Jul. 2018.
- [12] S. Kim, K. Park, and J. Seo, "Mitigation of GPS chirp jammer using a transversal FIR filter and LMS algorithm," in *Proc. ITC-CSCC*, 2019.
- [13] K. Park, D. Lee, and J. Seo, "Adaptive signal processing method using a single-element dual-polarized antenna for GNSS interference mitigation," in *Proc. ION GNSS+*, 2017, pp. 3888–3897.
- [14] S. Jeong, H. Lee, T. Kang, and J. Seo, "RSS-based LTE base station localization using single receiver in environment with unknown path-loss exponent," in *Proc. ICTC*, 2020, pp. 958–961.
- [15] H. Moon, H. Park, and J. Seo, "HELPS for emergency location service: Hyper-enhanced local positioning system," *IEEE Wirel. Commun.*, vol. 31, no. 4, pp. 276–282, 2024.
- [16] H. Lee and J. Seo, "Performance comparison of machine learning algorithms for received signal strength-based indoor LOS/NLOS classification of LTE signals," *J. Position. Navig. Timing*, vol. 11, no. 4, pp. 361–368, 2022.
- [17] Y. Jiao and Y. T. Morton, "Comparison of the effect of high-latitude and equatorial ionospheric scintillation on GPS signals during the maximum of solar cycle 24," *Radio Sci.*, vol. 50, no. 9, pp. 886–903, 2015.
- [18] K. Sun, H. Chang, J. Lee, J. Seo, Y. Jade Morton, and S. Pullen, "Performance benefit from dual-frequency GNSS-based aviation applications under ionospheric scintillation: A new approach to fading process modeling," in *Proc. ION ITM*, 2020, pp. 889–899.
- [19] J. Seo, T. Walter, and P. Enge, "Availability impact on GPS aviation due to strong ionospheric scintillation," *IEEE Trans. Aerosp. Electron. Syst.*, vol. 47, no. 3, pp. 1963–1973, Jul. 2011.

- [20] H. Lee, S. Pullen, J. Lee, B. Park, M. Yoon, and J. Seo, "Optimal parameter inflation to enhance the availability of single-frequency GBAS for intelligent air transportation," *IEEE Trans. Intell. Transp. Syst.*, vol. 23, no. 10, pp. 17 801–17 808, Oct. 2022.
- [21] A. K. Sun, H. Chang, S. Pullen, H. Kil, J. Seo, Y. J. Morton, and J. Lee, "Markov chain-based stochastic modeling of deep signal fading: Availability assessment of dual-frequency GNSS-based aviation under ionospheric scintillation," *Space Weather*, vol. 19, no. 9, pp. 1–19, Sep. 2021.
- [22] J. Lee, Y. Morton, J. Lee, H.-S. Moon, and J. Seo, "Monitoring and mitigation of ionospheric anomalies for GNSS-based safety critical systems," *IEEE Signal Process. Mag.*, vol. 34, no. 5, pp. 96–110, Sep. 2017.
- [23] N. Ahmed and J. Seo, "Statistical evaluation of the multi-frequency GPS ionospheric scintillation observation data," in *Proc. ICCAS*, 2017, pp. 1792–1797.
- [24] W. Kim, P.-W. Son, S. G. Park, S. H. Park, and J. Seo, "First demonstration of the Korean eLoran accuracy in a narrow waterway using improved ASF maps," *IEEE Trans. Aerosp. Electron. Syst.*, vol. 58, no. 2, pp. 1492–1496, Apr. 2022.
- [25] J. H. Rhee, S. Kim, P.-W. Son, and J. Seo, "Enhanced accuracy simulator for a future Korean nationwide eLoran system," *IEEE Access*, vol. 9, pp. 115 042–115 052, Aug. 2021.
- [26] P.-W. Son, S. G. Park, Y. Han, and K. Seo, "eLoran: Resilient positioning, navigation, and timing infrastructure in maritime areas," *IEEE Access*, vol. 8, pp. 193 708–193 716, 2020.
- [27] P.-W. Son and T. H. Fang, "Enhancing coastal air navigation: eLoran 3D positioning and cycle slip mitigation," *IEEE Access*, vol. 12, pp. 100 230–100 239, 2024.
- [28] P.-W. Son, S. G. Park, Y. Han, K. Seo, and T. H. Fang, "Demonstration of the feasibility of the Korean eLoran system as a resilient PNT in a testbed," *Remote Sens.*, vol. 15, no. 14, pp. 1–12, 2023.
- [29] P.-W. Son, T. H. Fang, S. Park, Y. Han, , and K. Seo, "Compensation method of eLoran signal's propagation delay and performance assessment in the field experiment," *J. Position. Navig. Timing*, vol. 11, no. 1, pp. 23–28, 2022.
- [30] P.-W. Son, Y. Han, K. Seo, and T. H. Fang, "Analysis of range measurement based on MF DGNSS infrastructures," *J. Position. Navig. Timing*, vol. 11, no. 4, pp. 245–250, 2022.
- [31] —, "Development of MF R-Mode transmitting system for maritime resilient PNT in the Republic of Korea," *J. Position. Navig. Timing*, vol. 11, no. 4, pp. 239–244, 2022.
- [32] J. Yu and J. Rhee, "Simulation of medium-frequency R-Mode signal strength," in *Proc. IEEE ICCE-Asia*, 2022.
- [33] J. Yu and P.-W. Son, "Empirical modeling of variance in medium frequency R-Mode time-of-arrival measurements," in *Proc. ICCAS*, 2023.
- [34] S. C. Lo, B. B. Peterson, and P. K. Enge, "Loran coverage availability simulation tool," in *Proc. ION GNSS*, September 2008, pp. 2595–2605.